

Remarks

Claims 1-10, 18-25, and 28-34 were pending in the subject application. Claims 5, 7, 22, 23, and 25 remain pending but withdrawn from consideration. Submitted herewith is a Request for Continued Examination (RCE) under 37 CFR §1.114 for the subject application. By this Amendment, claims 6, 7, 24, and 25 have been amended. Support for the amendments can be found throughout the subject specification and in the claims as originally filed. Entry and consideration of the amendments presented herein is respectfully requested. Accordingly, claims 1-4, 6, 8-10, 18-21, 24, and 28-34 are currently before the Examiner for consideration. Favorable consideration of the pending claims is respectfully requested.

Claims 30-34 are rejected under 35 USC §112, first paragraph, as lacking adequate written description, and under 35 USC §112, second paragraph, as indefinite. The Examiner objects to the language “root of said dendrimer” in the claims. The Examiner asserts that the subject specification does not provide adequate support for the claim language and that use of the term “root” renders the claims indefinite. Applicants respectfully assert that there is support for the claim language and that the claims as filed are definite. It is well accepted in the scientific literature on dendrimers that dendrimers have a “tree like” structure, *e.g.*, root and branches (see *e.g.*, N. Zacharopoulos and I. G. Economou, *Macromolecules*, 2002, 35:1814-1821). In fact, the word dendrimer comes from the Greek word “dendron” meaning “tree.” Applicants also respectfully disagree with the Examiner’s assertion that the root can be any anchor point on the dendrimer. In dendrimer literature, “root” has a specific meaning and pertains to the dendrimer core (*i.e.*, the origin of the branching structure).

The Examiner asserts under the written description rejection that the specification only describes the “root” of dendritic reagents. Applicants respectfully assert that this provides support for root of a dendrimer. The dendritic reagent is used to prepare the dendrimer and shares structure with it. Thus, the “root” of a dendritic reagent would be understood by the ordinarily skilled artisan to also refer to the “root” of the dendrimer. It is well settled in patent law that the language used in an amendment of a claim does not have to be disclosed word for word in a specification. *In re Wilder*, 222 USPQ 369, 372 (Fed. Cir. 1984) (“It is not necessary that the claimed subject matter be described identically, but the disclosure must convey to those skilled in the art that applicant had

invented the subject matter later claimed.”); *In re Lukach*, 169 USPQ 795, 796 (CCPA 1971) (“... the invention claimed does not have to be described in *ipsis verbis* in order to satisfy the description requirement of §112.”). In addition, the Patent Office guidelines for examiners make it clear that explicit written support is not required to meet the requirements of 35 USC § 112, first paragraph. (“To comply with the written description requirement of 35 U.S.C. §112, ¶ 1, ... each claim limitation must be expressly, **implicitly**, or **inherently** supported in the originally filed disclosure.” (emphasis added) See “Guidelines for Examination of Patent Applications Under 35 U.S.C. §112, ¶ 1, ‘Written Description’ Requirement,” *Federal Register* Vol. 66, No. 4, pp. 1099-1111, at page 1107, first column, lines 10-17). Thus, support for a claim limitation can be implicit or inherent in the disclosure of a patent application. Applicants respectfully assert that there is both explicit and implicit support in the specification for the term “root of said dendrimer moiety.” Accordingly, reconsideration and withdrawal of the rejections under 35 USC §112, first and second paragraphs, is respectfully requested.

Claims 1-4, 8-10, 18-21, and 28 are rejected under 35 USC §103(a) as obvious over Malik and Wang (WO 00/11463) in view of either Kim *et al.* (U.S. Published Application No. 2002/0020669) or Neumann *et al.* (German Patent No. DE 19,621,741) and the PTO 03-679 translation of Neumann *et al.* (German Patent No. DE 19,621,741). In addition, claims 6, 7, 24, 25, and 29-34 are rejected under 35 USC §103(a) as obvious over Malik and Wang (WO 00/11463) in view of either Kim *et al.* (U.S. Published Application No. 2002/0020669) or Neumann *et al.* (German Patent No. DE 19,621,741) and the PTO 03-679 translation of Neuman *et al.* (German Patent No. DE 19,621,741) and further in view of Newkome *et al.* (U.S. Patent No. 5,703,271). Applicants traverse these grounds of rejection.

Applicants respectfully assert that the claimed invention is not obvious over the cited references, regardless of whether the references are taken alone or in combination. The present invention is not obvious over the cited references since conventional dendrimers lack a sol-gel-active root. If a person were to use a conventional dendrimer (*i.e.*, one without a sol-gel-active root in its structure) in the sol-gel system taught by Malik and Wang (WO 00/11463), the dendrimer will not chemically bond to the sol-gel matrix. A capillary column coated with such a sol-gel matrix will not

be effective as a stationary phase or as an extraction medium since the dendrimer molecules will be washed off the capillary column during any rinsing with solvents.

As noted above, conventional dendrimers do not possess a sol-gel active root and none of the cited references teach how to prepare dendrimer with a sol-gel active root. Applicants note that the Neumann *et al.* patent first derivatizes the silanol groups on a silica surface with sol-gel-inactive groups (e.g., amine) leaving essentially no accessible silanol groups to participate in the sol-gel reactions for covalent attachment of the sol-gel dendrimer coating to the silica surface. Therefore, if the teachings of the Malik and Wang publication is applied to the derivatized surface of the Neumann *et al.* patent, the created sol-gel coating will not be chemically bonded to the fused silica surface (few accessible silanol groups after derivatization) resulting in an unstable coating which will be easily washed off the substrate during treatment or operation. Clearly, a person of ordinary skill in the art having considered the cited references would not arrive at the sol-gel dendrimer capillary of the present invention where the sol-gel dendrimer coating is covalently bonded to the sol-gel substrate on the fused silica capillary surface.

The Kim *et al.* publication derivatizes the dendrimer's exterior functional sites – not the root. If the dendrons of Kim *et al.* (with derivatized exterior functional sites) are used to prepare a sol-gel dendron capillary column following the teachings of Malik and Wang, it will lead to one of the following two outcomes depending on whether the derivatized arm of the dendrimer is sol-gel-active or not:

(1) If the derivatized arm of the dendron is not sol-gel active, it will lead to a capillary column where the dendron is not chemically bonded to the sol-gel substrate of the created stationary phase coating, and therefore, this physically held dendron will be easily washed off or lost during capillary preparation, conditioning, or operation.

(2) If the derivatized arm of the dendron is sol-gel active, it will lead to a stationary phase where the dendron is attached to the sol-gel substrate by the crown (not by the root) since the derivatization is carried out on the exterior functional sites. Such architecture of the sol-gel dendron stationary phase is undesirable since it will drastically reduce the number of terminal functional groups on the dendron available for interaction with the analyte molecules. This is in direct contrast with the present invention where the dendron can be chemically attached to the sol-gel substrate by

the root, thereby exposing all the terminal functional groups on the dendron for effective interaction with the analyte molecules. Thus, a person of ordinary skill in the art would not arrive at Applicants' claimed invention when considering the teaching of Malik and Wang in conjunction with the teaching of the Kim *et al.* publication.

The Examiner states that the word "crown" does not appear in the Kim *et al.* publication. It is evident through the disclosure in the Kim *et al.* publication that the point of attachment is through that portion of the dendrimer known in the art as the "crown" of the dendrimer. As Applicants have explained, the structure of a dendrimer can be described using well-accepted terms in the dendrimer art. "Crown" is one such term. The molecular structure of a dendrimer as understood in the dendrimer art was discussed in Applicants' Amendment dated January 14, 2008. Thus, it is irrelevant that the word "crown" does not appear in the Kim *et al.* publication. A person of ordinary skill in the dendrimer art would understand the meaning of the term and would understand that in the Kim *et al.* publication, the point of attachment is through the dendrimer crown.

The Examiner further asserts in the Office Action that the word "root" is not considered to be specific to any particular orientation. As noted previously herein, the term "root" does not apply to "any point" of attachment of the dendrimer to the sol-gel. Rather, the term "root" refers to a specific part of the dendrimer structure.

The Examiner further asserts in the Office Action that "page 9, line 10 of the remarks would appear to ascribe a more particular meaning to root because conventional dendrimers lack applicants' particular root." The Examiner concludes that the "specification lacks support for both roots in general and particular roots." Applicants are unclear as to what point the Examiner is making and how it relates to the obviousness rejection.

Applicants respectfully assert that the Newkome *et al.* patent does not cure the deficiencies of the Malik and Wang publication, the Neumann *et al.* patent or the Kim *et al.* publication. The Newkome *et al.* patent does not teach or suggest how to chemically bind an isocyanate monomer-based dendron to a sol-gel substrate by the dendron root. Thus, the Newkome *et al.* patent suffers from the same failings as the Neumann *et al.* patent and the Kim *et al.* publication.

In addition, Applicants note that the methods described by Neumann *et al.* and Kim *et al.* for the preparation of dendrimer stationary phases are lengthy, requiring days and even months as

opposed to a few hours required by the present invention. For example, on page 7 of the English translation of Neumann *et al.*, the author describes a method that requires 50 (fifty) days just to complete the chemical reactions for the preparation of a dendrimer stationary phase. Additional time will be required for washing, drying, packing, and conditioning of the stationary phase particles. By comparison, the present invention requires only a few of hours for the preparation of a capillary column from start to finish (including *in situ* synthesis of the sol-gel dendrimer stationary phase, covalent binding of the stationary phase onto the inner walls of a fused silica capillary as well as washing, purging, and thermal conditioning of the coated stationary phase).

As the Examiner is aware, it is well established in patent law that in order to support a *prima facie* case of obviousness, a person of ordinary skill in the art must generally find both the suggestion of the claimed invention, and a reasonable expectation of success in making that invention, solely in light of the teachings of the prior art and from the general knowledge in the art. *In re Dow Chemical Co.*, 5 USPQ2d 1529, 1531 (Fed. Cir. 1988). One finds neither the suggestion, nor the reasonable expectation of success, of Applicants' claimed invention in the cited references. Accordingly, reconsideration and withdrawal of the rejections under 35 USC §103(a) is respectfully requested.

It should be understood that the amendments presented herein have been made solely to expedite prosecution of the subject application to completion and should not be construed as an indication of Applicants' agreement with or acquiescence in the Examiner's position.

In view of the foregoing remarks and amendments to the claims, Applicants believe that the currently pending claims are in condition for allowance, and such action is respectfully requested.

The Commissioner is hereby authorized to charge any fees under 37 CFR §§1.16 or 1.17 as required by this paper to Deposit Account 19-0065.

Applicants invite the Examiner to call the undersigned if clarification is needed on any of this response, or if the Examiner believes a telephonic interview would expedite the prosecution of the subject application to completion.

Respectfully submitted,



Doran R. Pace  
Patent Attorney  
Registration No. 38,261  
Phone No.: 352-375-8100  
Fax No.: 352-372-5800  
Address: Saliwanchik, Lloyd & Saliwanchik  
A Professional Association  
P.O. Box 142950  
Gainesville, FL 32614-2950

DRP/mv

Attachments: Request for Continued Examination

Zacharopoulos and Economou, *Macromolecules*, 2002, 35:1814-1821

## Morphology and Organization of Poly(propylene imine) Dendrimers in the Melt from Molecular Dynamics Simulation

Nikolas Zacharopoulos and Ioannis G. Economou\*

Molecular Modelling of Materials Laboratory, Institute of Physical Chemistry, National Research Centre for Physical Sciences "Demokritos", GR-15310 Aghia Paraskevi Attikis, Greece

Received June 1, 2001; Revised Manuscript Received November 1, 2001

**ABSTRACT:** Molecular dynamics simulations are performed on generations 2 (G2) through 5 (G5) of poly(propylene imine) dendrimers at 400 K in order to investigate characteristics of molecular structure and morphology in the melt. As the generation increases, the dendrimers assume a more spherical shape, and the degree of dendron overlap increases, albeit at a decaying rate. The distribution of end groups within the molecule widens with *G* and separates at G5 into inner (back-folded), intermediate, and outer rims. Back-folded branches are accommodated by the increased extension of the initial spacers. Furthermore, the radius of gyration scales approximately with the cubic root of the number of monomers. Finally, interpenetration of individual dendrimer molecules decreases with generation. Simulation results are in good agreement with the limited experimental data available.

### Introduction

Dendrimers are highly ordered, well-defined branched polymers, with segments between branch points (spacers) comprising relatively short chains. Their treelike structure is formed by a stepwise, iterative reaction sequence of the functional groups in each generation starting from and radiating out from a smaller, multifunctional initiator core molecule from which the main branches or dendra emanate.<sup>1,2</sup> When the recursive process leads to complete shells for each generation, monodisperse polymers are fabricated that have a defined number of end groups, and their size and architecture are specifically controlled in the synthesis. Dendrimers find potential use in nanoscale catalysis, as micelle mimics, supramolecular building blocks, molecule encapsulation and delivery agents, etc.<sup>3</sup> A key aspect in all these applications is the understanding of the molecular structure, particularly the end group distribution within the dendrimer molecule, information needed to guide the design and synthesis.

The location of the terminal groups has been a point of controversy in the literature starting with the study of de Gennes and Hervet<sup>4</sup> who made the assumption of fully extended branches with the end groups on the periphery of the molecule predicting a limiting generation due to steric hindrance. The congestion at the surface is due to the fact that the number of end groups grows exponentially with generation while the surface of the molecule increases as the radius (proportional to the generation in the fully extended model) squared. The picture of the end groups lying on the periphery is supported by X-ray scattering experiments;<sup>5</sup> however, studies based solely on radius of gyration data have been shown to be inconclusive.<sup>6</sup> In addition, resonance techniques are limited in their ability to resolve the resonances from the many unique but very similar groups in the molecule. So far, conventional 1-d NMR data<sup>7,8</sup> have provided evidence of proximity of the terminal groups to the dendrimer core. Recently, a 3-d

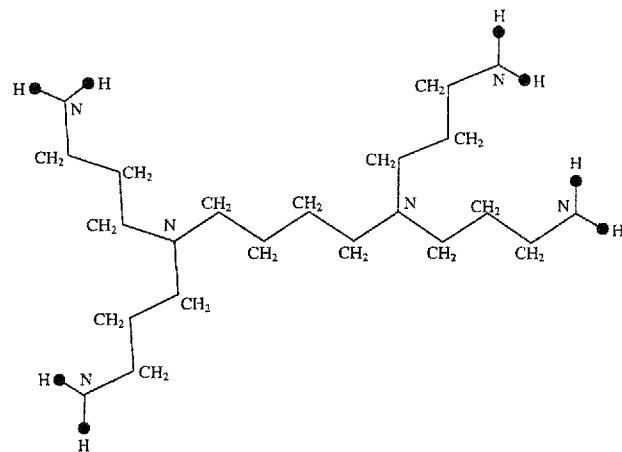


**Figure 1.** Schematic representation of the model PPI G1 dendrimer. The methylene groups are treated as united atoms.

NMR technique was used to separate the overlapping H resonances from the core, interior and exterior methylene groups of third generation poly(propylene imine) (PPI) dendrimers,<sup>9a</sup> thereby allowing for experimental data on the arrangement of dendra without the need to resort to isotopic labeling. Using this technique, it was shown that PPI dendrimers assume different conformations in polar and nonpolar solvents.<sup>9b</sup> Simulations and theoretical models applied to dendrimer solutions, for the most part, produce an even distribution of end groups throughout the molecule and a density profile that decreases outward from the core.<sup>10–15</sup>

In the present study, we investigate the structural features of a widely studied and commercially available dendrimer, namely PPI formed of a binary core of 1,4-diaminobutane, to obtain detailed information on the size and internal organization of the molecule. To this end, we employ molecular dynamics (MD) simulations of the dendrimer in the molten state, using an atomistic force field to account for the interactions. To our knowledge, this is the first published work on atomistic simulation of dendrimer melts. Melt properties will be used as reference in future studies of solution properties for the same dendrimer in different solvents.

\* Corresponding author. E-mail: economou@mistras.chem.demokritos.gr. Telephone: ++ 30 1 6503963. Fax: ++ 30 1 6511766.

Table 1. Parameters of the DREIDING Force Field<sup>16</sup> for the Atoms Examined in This Work

atom type i	bond stretching <sup>a</sup>		bond bending <sup>b</sup>		Lennard-Jones <sup>c</sup>	
	$b_i^0$ (Å)	$k_{b_i}$ (kcal/mol/Å <sup>2</sup> )	$\theta_i^0$ (deg)	$k_{\theta_i}$ (kcal/mol/rad <sup>2</sup> )	$\sigma_i$ (Å)	$\epsilon_i$ (kcal/mol)
H	0.330	700	180.0	100/(sin $\theta_i^0$ ) <sup>2</sup>	3.1950	0.0152
N	0.702	700	106.7	100/(sin $\theta_i^0$ ) <sup>2</sup>	3.6621	0.0774
CH <sub>2</sub>	0.770	700	109.471	100/(sin $\theta_i^0$ ) <sup>2</sup>	4.0677	0.1984

<sup>a</sup>  $b_{ij}^0 = b_i^0 + b_j^0 - \delta$ ;  $\delta = 0.01$  Å. <sup>b</sup> For  $\theta_i^0 = 180^\circ$ , the bending term in eq 1 is  $k_{\theta_i}(1 + \cos \theta_i)$ ;  $k_{\theta_i} = 100$  kcal/mol/rad<sup>2</sup>. <sup>c</sup>  $\epsilon_{ij} = (\epsilon_i \epsilon_j)^{1/2}$ ;  $\sigma_{ij} = (\sigma_i + \sigma_j)/2$ . Torsion: sp<sup>3</sup>–sp<sup>3</sup>:  $k_{\phi_i} = 2.0$  kcal/mol,  $n_i = 3$ ,  $\phi_i^0 = 180^\circ$ . sp<sup>3</sup>–sp<sup>2</sup>:  $k_{\phi_i} = 1.0$  kcal/mol,  $n_i = 6$ ,  $\phi_i^0 = 0^\circ$ .

## Simulation Details

All simulations presented in this work were performed using the Cerius<sup>2</sup> software package of Accelrys Inc. (previously known as Molecular Simulations Inc.). Figure 1 shows a schematic representation of the molecular model for a first generation PPI dendrimer. The DREIDING force field<sup>16</sup> was used to describe the intra- and intermolecular interactions. It has the following general form:

$$E = \frac{1}{2} \sum_i^{\text{all bonds}} k_{b_i} (b_i - b_i^0)^2 + \frac{1}{2} \sum_i^{\text{all angles}} k_{\theta_i} (\cos \theta_i - \cos \theta_i^0)^2 + \frac{1}{2} \sum_i^{\text{all torsional angles}} k_{\phi_i} \{1 - \cos[n_i(\phi_i - \phi_i^0)]\} + \sum_{i,j}^{\text{all non-bonded sites}} \epsilon_{ij} \left[ \left( \frac{\sigma_{ij}}{r_{ij}} \right)^{12} - 2 \left( \frac{\sigma_{ij}}{r_{ij}} \right)^6 \right] \quad (1)$$

The first three terms in the sum account for bond stretching, bond bending, and dihedral angle rotation around the equilibrium values  $b^0$ ,  $\theta^0$ , and  $\phi^0$ , respectively. The last term accounts for the nonbonded dispersion interactions expressed by the Lennard-Jones potential; a cutoff distance of 1.0 nm is used, with a cut-in distance for a spline switching method set to 0.9 nm. The constants and geometric parameters in DREIDING are defined with consideration to the hybridization of the atom types rather than the specific combination of atoms. In this work, methylene groups are treated as united atoms. This approach reduces the computational time significantly without reducing the accuracy of the calculations. The constants and parameters for the relevant atom types are presented in Table 1. Periodic boundary conditions were used to simulate the melt, with the system size kept at around 2500 interaction sites. In this way, melts of 36, 17, 8, and 4 molecules were examined for generations 2, 3, 4, and 5, respectively. The initial system density was chosen to be 1.06 g/cm<sup>3</sup>, yielding a simulation cell edge of about 25 Å.

In all cases, the energy was initially minimized using a hundred steps of steepest descent followed by 4000–5000 steps of conjugate gradient to relax the structure. The melt was then subjected to MD simulated annealing of five repeat cycles from 400 to 700 K and back, in steps of 50 K, spending 2 ps in each step under *NPT* conditions (with pressure equal to 1 atm) to release the molecules from potential configurational traps or initial biases. The energy was minimized at the end of each annealing cycle via molecular mechanics. The ensuing *NPT* MD simulation consisted of a 100 ps long equilibration run, followed by a data collection run of 400 ps at 400 K and 1 atm. The integration time step was chosen to be 1 fs while trajectory data were stored every

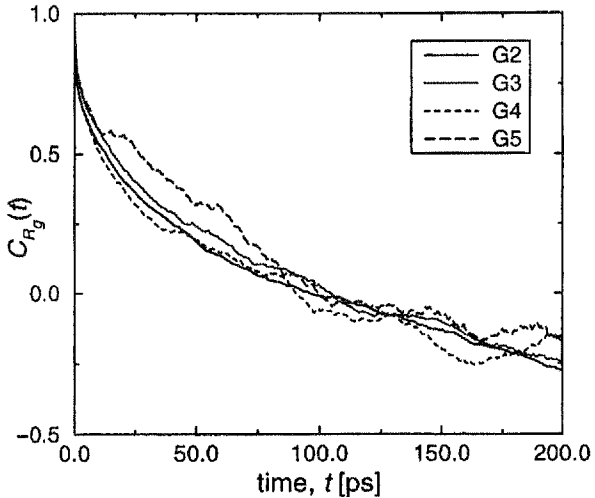


Figure 2. Autocorrelation function of the squared radius of gyration.

100 time steps. The simulations proceeded at a rate of approximately 14 min of CPU time for each simulated ps on a SGI Indigo2 R10000 processor at 195 MHz.

## Results and Discussion

The relaxation process described above resulted in stabilizing the energy and the radius of gyration,  $R_g$ , of the dendrimer, averaged over all molecules. Equilibrium values were reached within the first 50 ps. To examine the relaxation of dendrimer molecules, the autocorrelation function of the squared radius of gyration,  $C_{R_g}(t)$ , was evaluated from the expression:

$$C_{R_g}(t) = \frac{\langle (R_g^2(t) - \langle R_g^2 \rangle)(R_g^2(0) - \langle R_g^2 \rangle) \rangle}{\langle R_g^4 \rangle - \langle R_g^2 \rangle^2} \quad (2)$$

Results are shown in Figure 2 for the four generations considered. From these data, a relaxation time,  $t_{R_g}$ , where  $C_{R_g}(t_{R_g}) = 1/e$ , is calculated. The  $t_{R_g}$  values calculated were 24 ps for G2, 29 ps for G3, 20 ps for G4 and 45 ps for G5 dendrimer. With the exception of G4, we observe that, the relaxation time increases with the generation, in accordance also with previous simulation studies.<sup>11</sup> G4 represents the threshold generation of extended growth of the branches, with enough space available for large-scale maneuvering and subsequent resizing, as will be further elaborated later on.

MD simulations by Murat and Grest<sup>11</sup> for dendrimer solutions where the solvent was of varying quality resulted in relaxation times for G5 dendrimers in the range 25–70 τ, going from poor to athermal solvent, where  $\tau = \sigma(m/e)^{1/2}$  is the natural time unit. Substitution of the average values for  $\sigma$ ,  $m$ ,  $\epsilon$  for the atom types in the model considered here yields a relaxation time of 45–125 ps. Although quantitative comparison is not

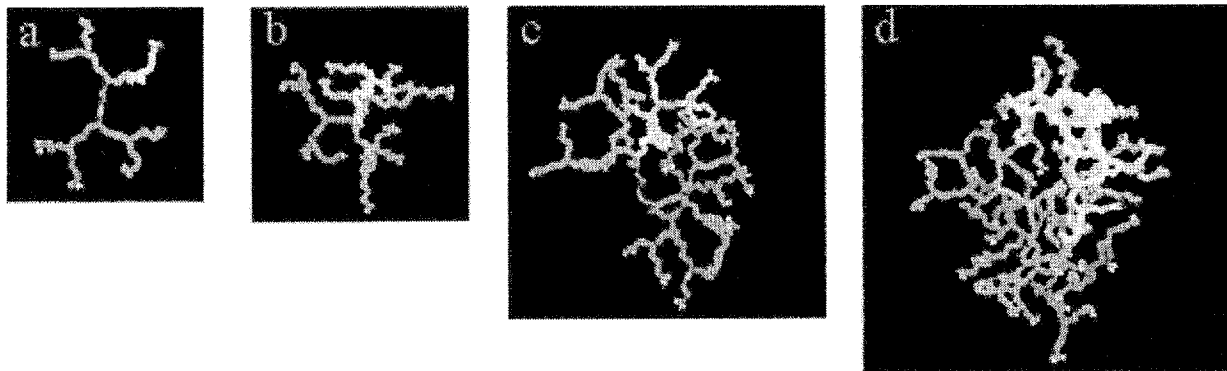


**Figure 3.** Typical equilibrated ( $t = 500$  ps) conformations of generations  $G2$  through  $G5$ . The colors represent the four dendra emanating from the gray core. The terminal hydrogens are depicted white.

possible because the molecular model used by Murat and Grest is different than the model used here, the agreement between the two sets of simulation is considered acceptable.

For all the systems examined here, the production run was divided into blocks of 80 ps. In the figures that follow, the data points represent the average and the error bars the standard deviation of the five blocks. The values reported here correspond to averages over all dendrimers included in the melt of the respective generation.

Typical equilibrated conformations of the four dendrimer generations examined here are shown in Figure 3. The different colors represent the four dendra stemming from the two ends (roots) of the dendritic core (gray), whereas the hydrogens of the end-groups are depicted white. As the generation number increases the molecule becomes more compact, and the dendra, subdendra, etc. turn inward, exhibiting a behavior fundamentally different from that observed for the lower generations characterized by extended branches. In addition, beyond the second generation there is a departure from the nearly two-dimensional shape, progressing from a tetrahedral (at the third generation) toward a more spherical spatial organization at the higher generations. The change in shape is reflected on the relative shape anisotropy,  $\kappa^2$ , defined as<sup>17</sup>

$$\kappa^2 = 1 - \frac{3I_2}{I_1^2} \quad (3)$$

where  $I_1$  and  $I_2$  are the first and second invariants of the radius of gyration tensor. This quantity assumes values between 1 (for a linear array of atoms) and 0 (for shapes of high 3-d symmetry). As shown in Figure 4, this quantity equals approximately 0.22 ( $\kappa^2 = 1/4$  for planar arrays) for second generation dendrimers and progressively decreases for higher generations (except for a small rise at  $G4$ , within the statistical uncertainty).

The overall dendrimer shape is inherently linked to the arrangement of the dendra within the molecule. To elucidate the internal structure of the dendrimers, we first analyzed their local conformation by examination of the dendron expansion pattern. More specifically, we measured the relative expansion,  $S$ , of sequential spacers by taking the projection of spacer vector  $\mathbf{I}_{m+1}$  on spacer vector  $\mathbf{I}_m$  (as defined graphically in the inset of Figure 5), where  $m$  and  $m + 1$  are sequential branch points, normalized by the theoretical spacer length,  $I$ ,

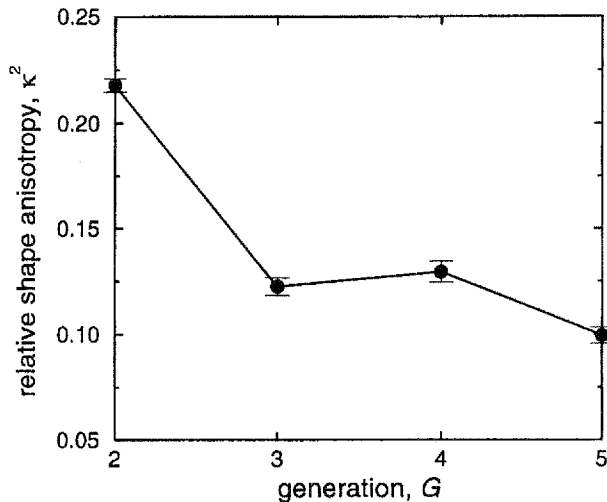


**Figure 4.** Relative shape anisotropy (see text) as a function of dendrimer generation.

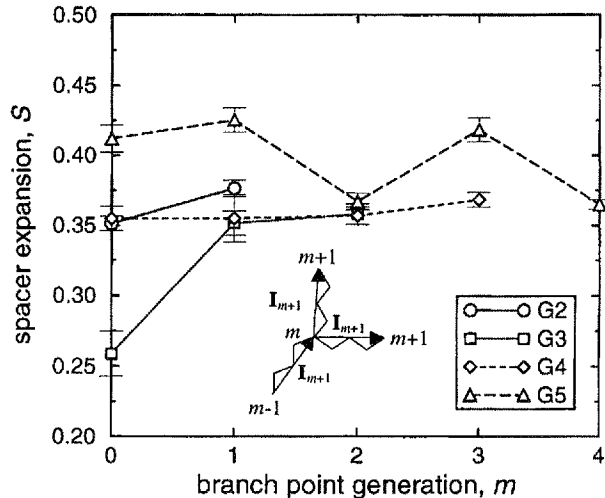


**Figure 5.** Spacer expansion,  $S$ , defined as the projection of vector  $\mathbf{I}_{m+1}$  on vector  $\mathbf{I}_m$ , normalized by the all-trans spacer length, as function of branch point generation,  $m$ , for  $G2$  through  $G5$ .

in an all-trans conformation (0.489 nm in this case):

$$S = \frac{\mathbf{I}_{m+1} \cdot \mathbf{I}_m}{|\mathbf{I}_m| I} \quad (4)$$

The spacer expansion, incorporating the effects of bond and torsional angles and of bond length on spacer

expansion, is plotted against the index of the common branch point, identifying the generation number  $m$  within the dendrimer, or the topological distance (in spacers) of the branch point from the respective root. Vector  $\mathbf{I}_0$  is the end-to-end vector of the initiator core molecule, and its direction is taken such that it is always in a head-to-tail connection with the respective  $\mathbf{I}_1$ . A similar analysis has been performed in the theoretical study of Ganazzoli et al.<sup>15</sup> for dendrimer solutions based on a more coarse-grained model than the one here, that is freely jointed chains. The local conformation in their case was expressed as the scalar product of sequential bond vectors of unit length in a head-to-tail connection ( $\langle \mathbf{I}_m \cdot \mathbf{I}_{m+1} \rangle$ ). In this theoretical treatment, a parabolic expansion was found for the case of a one-bond long spacer, with a maximum at  $m = 1$  or  $m = 2$  displaced to larger values along the ordinate with generation number  $G$  due to increased crowding of the end groups. This regular picture of expansion is largely owed to the stiff bonds connecting consecutive branch points and, as an average trend, persists even in the case of the slightly less rigid two-bond-long spacer.

The results of Figure 5 show the departure from regularity due to the highly flexible four-bond spacers. In all but the highest generation  $G$ , the expansion shows a relative increase as we move up the dendron in generation  $m$ , as spacers are forced to expand in a more confined environment. This is in agreement with the general concept of de Gennes and Hervet in which the spacers closer to the core are less extended than the ones near the periphery<sup>4</sup> (however, in our case, the proximity is topological not spatial). Moreover, the values for the three lower generations  $G$  are very close (hinting to similar internal structure). The only anomaly observed is in the low expansion of the first spacer of  $G3$ . Steric congestion on the plane forces the third generation to expand into the third dimension which for this generation is considerably open. The dendrimer assumes a structure that resembles a tetrahedron by torsion of the bonds in the first spacer. This shape, observed elsewhere in the literature,<sup>18,19</sup> brings apart most efficiently branch points of higher  $m$ . In generation  $G4$ , the tetrahedral organization leads to crowding, and higher symmetry structures are formed, characterized by an even distribution of spacer expansion along the dendron. Extended spread of dendra is no longer sustainable in  $G5$  dendrimers, thus producing a back-folding which is manifested as bending at the branch points of  $m = 2$  and  $m = 4$ . This behavior is readily visible in the conformation of  $G5$  of Figure 3 by tracing the succession of spacers leading from the core to the terminal group depicted orange. The initial spacer assumes a more extended conformation than at lower  $G$ , thereby forming an inner cavity where the back-folded branches are accommodated.

The spatial arrangement of branch points as a function of their topological distance from the respective root is presented in Figure 6. For the lower dendrimer generations the rate at which the branch points expand from the center of mass as a function of branch point generation,  $m$ , shows an increase up to  $m = 2$  and then starts to drop. In the case of  $G5$  dendrimers this rate is a monotonically decreasing function of the topological distance. Furthermore, comparison of the curves of  $G2$  and  $G5$  alludes to similar extended growth of initial spacers relative to the more confined expansion of  $G3$  and  $G4$ . This extended organization in the case of  $G2$  is

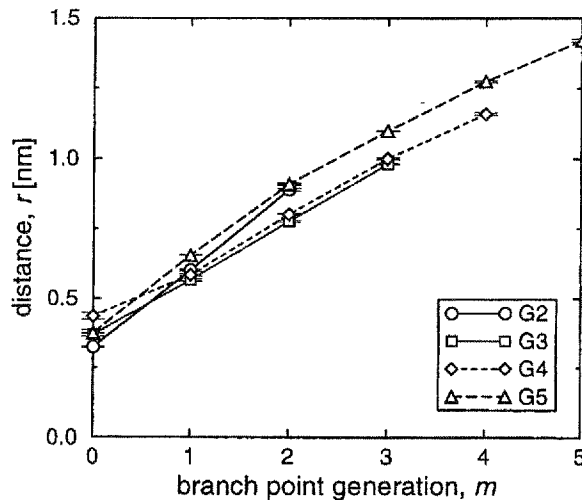


**Figure 6.** Branch point distance from the center of mass as a function of topological distance from the core for generations G2 through G5.

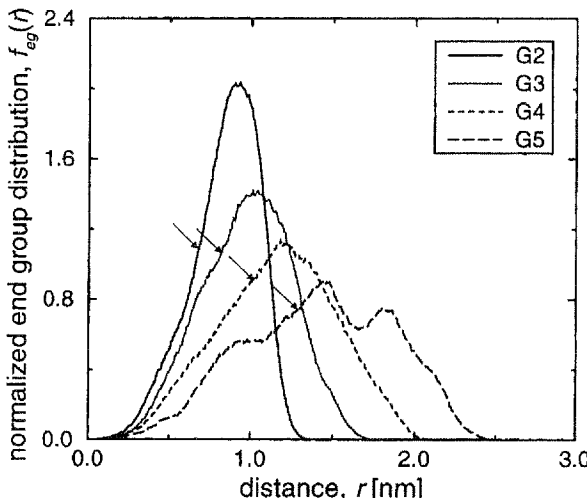


**Figure 7.** Normalized distribution of end groups as a function of distance from the center of mass for G2 through G5. The arrows point to the position of the radius of gyration of the respective dendrimer generation.

due to the absence of crowding, whereas in the case of  $G5$  it arises out of necessity for creating adequate available space to host the back-folded branches.

Further information on the arrangement of dendra within the dendrimer molecule can be obtained from the distribution of end groups, normalized by the number of end groups in each generation, as a function of core distance, presented in Figure 7. Going from the lowest to the highest generation, the end groups spread more uniformly over a widening range centered at an ever-decreasing distance from the radius of gyration of the dendrimer (marked with arrows). Moreover, the transition from extended to inward bent branches is evidenced by the change in distribution from unimodal at lower  $G$  to trimodal at  $G5$ . The bulk of the end groups is still inhabiting a shell in the vicinity of  $R_g$ , but there is considerable increase in their numbers at the periphery and in the inner regions of the dendrimer. Although dendrimers with  $G > 5$  were not investigated in the present study, we expect that, for higher generations the region around  $R_g$  will become depleted of end groups, giving rise to a bimodal distribution with end groups placed close to the core and on the surface of the

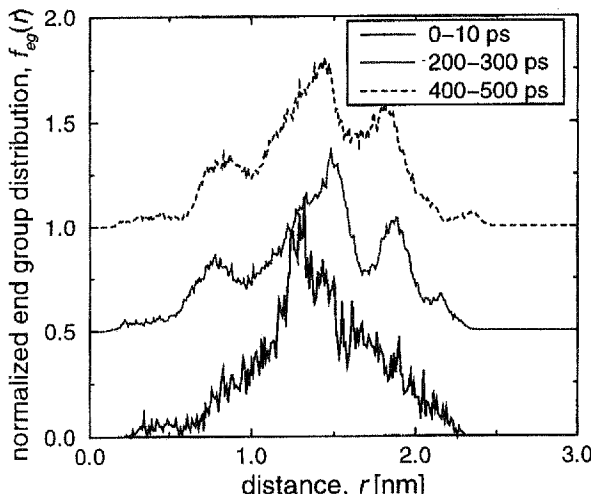


**Figure 8.** Normalized distribution of end groups for a single  $G_5$  dendrimer as a function of distance from the center of mass averaged over three separate periods of the simulation run. The curves are relatively displaced along the vertical axis by 0.5 for clarity.

molecule.<sup>20</sup> Figure 8 shows the distribution of end groups for a single  $G_5$  dendrimer averaged over the first 10, 200–300, and 400–500 ps. The three curves are relatively displaced along the ordinate by 0.5 for clarity. As the structure relaxes, the distribution departs from the energetically unfavorable high concentration around  $R_g$ , and the dendra self-organize into the trimodal state.

The radial number density distribution of the entire dendrimer molecule is depicted in Figure 9a. The density is calculated by drawing concentric spheres around the center of mass, incrementing the radius by 0.01 nm, and counting the number of segments within a spherical shell. The curve corresponding to  $G_2$  exhibits a monotonic decrease, briefly interrupted by a shoulder around the position of the  $m=0$  branch point (cf. Figure 6). The shoulder is revealing of the branched architecture and of the extended conformation of the dendra at  $G_2$ . The density for the higher generation dendrimers is characterized by a drop at distances very close to the center of mass, followed by a sharp rise. This behavior is due to the higher degree of space filling beyond  $G_2$ . The transition from the lower to the higher density values narrows and sharpens substantially at  $G_5$  as a consequence of back-folding. In addition, there is a region of small slope density drop, spread over the range of the first mode in the distribution of end groups (compare to Figure 7). The contribution of the final  $m$  generation to the overall density is readily captured in Figure 9b which shows the end group number density distribution. Finally, we note in Figure 9a that all  $G$ s seem to pass through the same density at around 0.167 nm, a value close to the theoretical bond length (0.153 nm).

The results for the complete density profile are in qualitative agreement with mean field models,<sup>21</sup> lattice<sup>12,13</sup> and hard sphere<sup>22</sup> Monte Carlo simulations, and coarse<sup>11</sup> and atomistic<sup>8,20,23</sup> MD simulations. All these studies predict that dendrimer density decays outward from the center of mass with terminal groups distributed all throughout the molecule. However, only the MD studies reported evidence of multimodal distribution of end groups. In most of the literature data above, the entire segment density of the terminal  $m$  generation was computed, rather than the isolated end group density

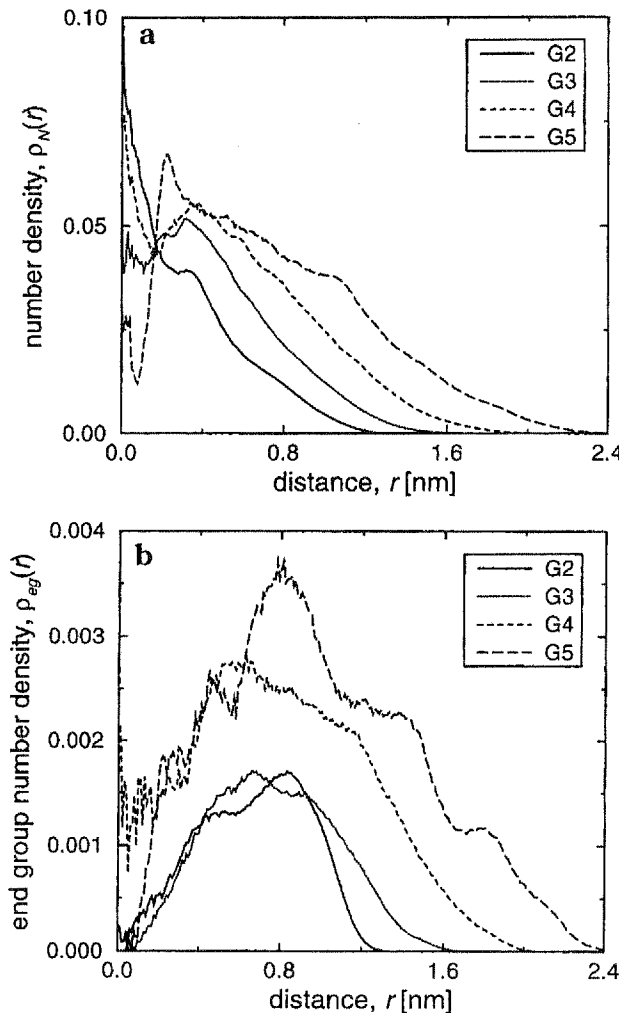


**Figure 9.** Radial number density distribution of (a) the entire molecule and (b) the end groups for generations  $G_2$  through  $G_5$ .

reported here. Therefore, inherent peaks in the density might have spread out over a wider range of distances accounting for the delocalized nature of an entire terminal spacer.

From the MD results, the amount of overlap of the four dendra within the dendrimer molecule was calculated. The dendrimer volume was divided into cubic cells of edge length 0.4 nm, with the origin placed at the center of mass. The occupancy of the cell identified by the indices  $i, j, k$  by an atom belonging to dendron  $\alpha$  ( $\alpha$  ranging from one to four) is defined as  $\psi_\alpha(i, j, k)$ , and can take the values 0 (unoccupied) or 1 (occupied). The total overlap,  $O_t$ , is determined from

$$O_t = \frac{2}{3} \sum_{\{i,j,k\}} \sum_{\alpha \neq \beta} \langle \psi_\alpha \psi_\beta \rangle \quad (5)$$

where the averages are over all configurations, and takes values between 0 and 1. This calculation is similar to a procedure introduced by Murat and Grest,<sup>11</sup> the main difference being that, in their work, averaging takes place outside the product. Averaging over the occupancy of a cell by each of the dendra separately and then calculating the product can lead to erroneous

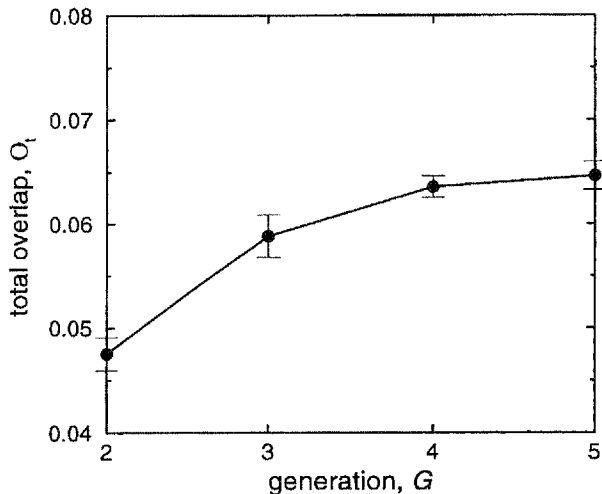


**Figure 10.** Total dendron overlap as a function of dendrimer generation.

results, since overlap is defined as the *simultaneous* occupancy of space: the occupancy events are *not* independent. The quantity described by eq 5 varies between complete overlap, when there is coexistence of all dendra contributing at least one atom each in every occupied cell, to complete segregation, when cell occupancy is owed exclusively to atoms of a single dendron. As shown in Figure 10, the overlap increases with  $G$ , and apparently reaches a plateau. This behavior is consistent with the picture of the dendrimer molecule assuming a compact spherical shape at higher generations, with the dendra interpenetrating at the surface ( $G4$ ) and/or close to the core because of back-folding ( $G5$ ). The trend followed here is the reverse of that observed by Murat and Grest for the case of dendrimer solutions,<sup>11</sup> mainly due to the difference in the methods used to calculate overlap. As the generation increases, the motion of individual dendra in an ever more confined environment leads to a decreased coverage of overall volume, i.e., to a decreased occupancy by each dendron. However, the number of cells that host segments of different dendra increases in denser surroundings; i.e., actual dendron overlap increases. Along the same lines, the conjecture by Mansfield<sup>24</sup> that dendra should overlap at the limiting generation, is corroborated by our results.

To locate dendron overlap within the molecule, we evaluated the radial overlap  $O(r)$  in a manner similar to  $O_t$  summing only over the cells that lie at a discrete distance  $r$  from the center of mass<sup>11</sup>

$$O(r) = \frac{2 \sum_{\{i,j,k\}} \sum_{\alpha \neq \beta} \langle \psi_\alpha \psi_\beta \rangle \delta_{r, r_{i,j,k}}}{3 \sum_{\{i,j,k\}} \sum_{\alpha = \beta} \langle \psi_\alpha \psi_\beta \rangle \delta_{r, r_{i,j,k}}} \quad (6)$$

This quantity is plotted in Figure 11 for the four generations examined. Moving toward the outside of the molecule the dendra become completely disentangled either monotonically with distance ( $G2, G3$ ), or with intermediate kinks at the periphery ( $G4$ ) and/or close to the core ( $G5$ ) corresponding to localized overlap. In particular, the low initial value of  $G5$  reflects the extended conformation of the  $m = 1$  spacer (cf. Figure 5), while the maximum overlap at this generation occurs

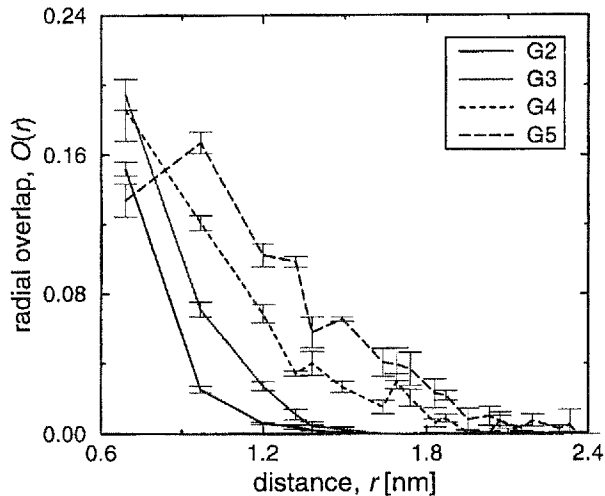


**Figure 11.** Radial dendron overlap for generations  $G2$  through  $G5$ .

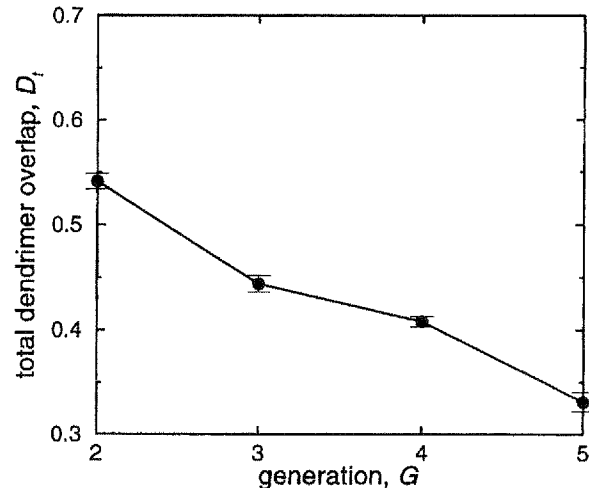


**Figure 12.** Total dendrimer overlap as a function of dendrimer generation.

around the first mode in the end group distribution where the density is highest (cf. Figures 7 and 9b).

The picture of overlap is completed with an analysis of the interpenetration of the dendrimer molecules. A method similar to the one described above was used, with total dendrimer overlap,  $D_t$ , being calculated by summation over all dendrimers of the averages of the product  $\psi_A \varphi_A$ , where  $\psi_A$  is the occupancy of a cell by dendrimer A and  $\varphi_A$  the occupancy of the same cell by *any* dendrimer *other* than A

$$D_t = \frac{\sum_{\{i,j,k\}} \sum_A \langle \psi_A \varphi_A \rangle}{\sum_{\{i,j,k\}} \sum_A \langle \psi_A \psi_A \rangle} \quad (7)$$

$\psi_A$  and  $\varphi_A$  are assigned the values 0 or 1 reflecting the absence or presence of dendrimer segments, respectively. The results of this analysis are depicted in Figure 12 as a function of the generation number. The trend followed is the reverse of that demonstrated by dendron overlap, with interpenetration decreasing with increasing generation. This result is expected on the basis of the previous discussion of dendrimer compactness at higher generations. Investigation of the localized den-

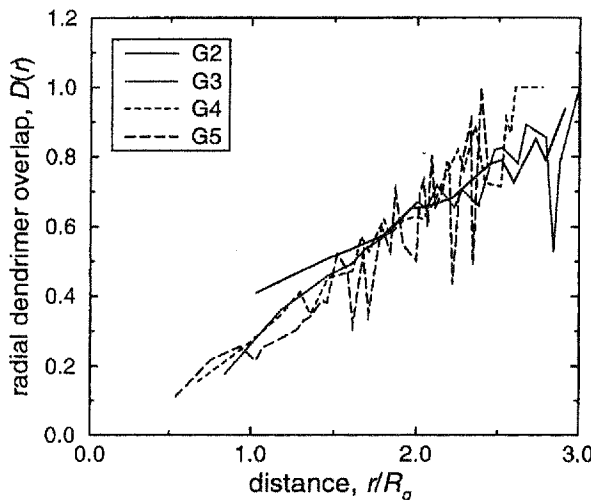


**Figure 13.** Radial dendrimer overlap for generations  $G_2$  through  $G_5$ .

dimer overlap as a function of the reduced distance from the center of mass of dendrimer A shown in Figure 13 reveals a very similar behavior for all generations, demonstrating a monotonic increase toward the periphery of the molecule. The higher value for  $G_2$  at small distances is owed to the considerably more open and nearly flat structure of the particular generation.

The dendrimer melt adapts well to the study of the scaling behavior as it produces conformations resembling the ones that result from the  $\Theta$  state. Chen and Cui,<sup>25</sup> who conducted Monte Carlo simulations on a model of freely rotating rigid bonds, observed that the scaling regime shrinks with increasing generation. They concluded that the correct scaling exponent for a high  $G$  dendrimer can, in fact, be obtained by reducing the effects of excluded volume (close to the  $\Theta$  point). Figure 14a shows the variation in the radius of gyration as a function of generation number compared to SANS data of PPI in 1% v/v in  $D_2O$ .<sup>20</sup> Although simulation results are generally in reasonable agreement with experimental data, the deviation from experiment increases with generation number in accord with the MD results by Scherrenberg et al.<sup>20</sup> The simulation data are plotted as a function of segment number,  $N$ , on a log-log scale in Figure 14b, along with the experimental results. The solid line is the best fit to a power law dependence with an exponent equal to 0.29. This scaling exponent, although higher than what is predicted by theory<sup>4,15</sup> and earlier simulation,<sup>10</sup> is in excellent agreement with the results of Mansfield and Klushin<sup>12</sup> (0.29 for their “augmented” dendrimers) and of Murat and Grest<sup>11</sup> (0.29 for  $T = \Theta$ ). Last, we note that the size of phantom dendrimers may be calculated analytically by means of the Wiener index.<sup>26</sup> This is a topological invariant of a molecular graph of  $n$  vertexes that is related to the unperturbed radius of gyration by  $W(n) = n^2 \langle R_g^2 \rangle^{1/2}$ , where  $l$  is the bond length. Using the analytical form of the Wiener index for *monocentric* dendrimers<sup>27</sup> together with an average value for the bond length, we estimate a dependence of the radius of gyration,  $R_g \propto N^{0.31}$ . The scaling exponent is very close to the value of 0.29 for our *dicentric* dendrimer for which the Wiener index differs only by a fairly constant multiplier.<sup>28</sup>

Finally, the fractal dimension of the dendrimer in each generation was calculated from its respective number density profile,  $\rho_N(r)$  (Figure 9a), using the

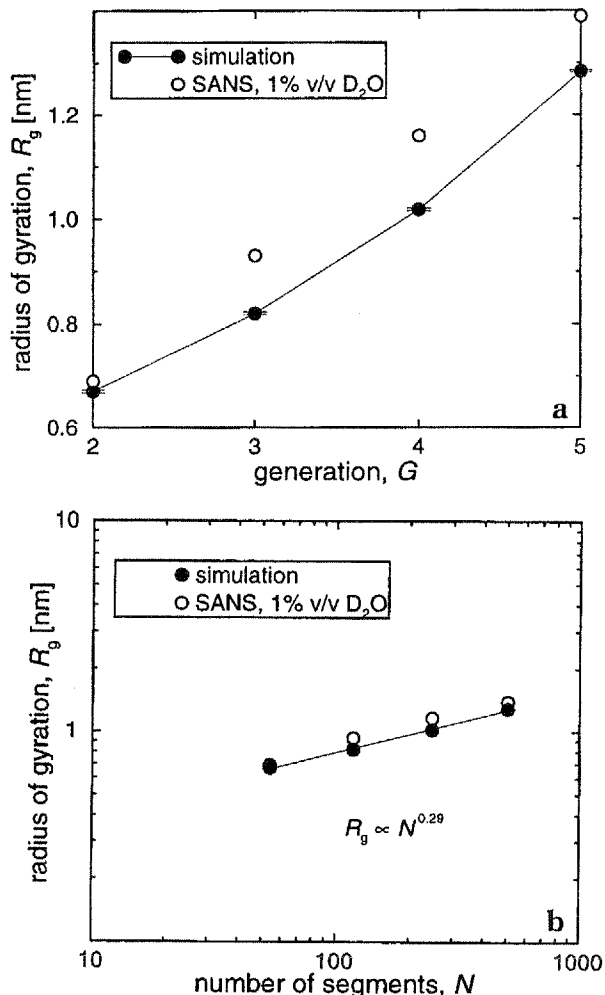


**Figure 14.** Experimental data<sup>20</sup> and simulation results for the PPI dendrimer radius of gyration as a function of (a) dendrimer generation, and (b) number of segments.

method suggested by Murat and Grest,<sup>11</sup> which relates the radial segment number,  $N(r)$ , with the distance from the center of mass

$$N(r) = 4\pi \int_0^r r'^2 \rho_N(r') dr' \quad (8)$$

The exponent extracted from a log-log plot of  $N(r)$  is 2.56, 2.95, 2.88, and 3.09 in order of increasing generation  $G$ . The relatively increased fractality at  $G_3$  is consistent with the results of Figure 4: the tetrahedral structure of these dendrimers allows them to fill space more effectively than their  $G_4$  counterparts. The fractal dimensions are presumably higher than those of Mansfield<sup>13</sup> (generations six through nine were reported) and closer to the ones calculated by Murat and Grest.<sup>11</sup> The value of 3.09 at  $G_5$  further supports the notion of a compact molecule at higher generations.

## Conclusions

We have performed molecular dynamics simulations on dendrimers of generations two through five in the molten state. The properties investigated aim at gaining insight on the internal organization of the dendritic molecule. In particular, the determination of spacer expansion demonstrates that there exists a critical generation ( $G_5$  in the case of PPI), at (and beyond) which the outward extended dendra of the lower gen-

eration dendrimers grow partially organized in a back-folded arrangement. The end group density distribution, which shows the reinforcement of the regions close to the center of mass and the periphery, completes a picture of dendrimers of higher generations comprising heavily extended and back-folded branches. We speculate that at the limiting generations the bimodal distribution prevails.

The overall density profiles exhibit a gradual decrease from the center of mass toward the surface of the molecule. At the critical generation where back-folding becomes evident, the density shows a sharp well near the core and a smooth decay on the molecular periphery, interrupted by a region of reduced slope. Related to the density is the entanglement of the dendra, which appears to grow with generation, albeit at an ever-decreasing rate, supporting the picture of a compact, space-filling molecule at the higher generations. Due to the higher degree of packing, interpenetration of individual molecules decreases with generation. Further evidence of space-filling is provided from the variation of the fractal dimension with generation reaching the spatial dimension for  $G_5$ . Finally, the molecule approaches a spherical shape as it grows in generation. Dendrimer size is shown to scale with the number of segments as  $N^{0.29}$ . Current work focuses on the structure and morphology of PPI in solution.

**Acknowledgment.** We are indebted to Professor Doros Theodorou for invaluable suggestions and discussions regarding this work. We thank Accelrys, Inc. for making their Polymer Consortium software available to the Molecular Modelling of Materials Laboratory through an agreement with Professor Doros Theodorou. Financial support of this work by the PENED-99 program of the Greek Secretariat of Research and Technology (GSRT) is gratefully acknowledged.

## References and Notes

- (1) Fréchet, J. M.; Hawker, C. J. In *Comprehensive Polymer Science*, 2nd suppl., Aggarwal, S., Russo, S., Eds.; Pergamon Press: Oxford, England, 1996; pp 234–298.
- (2) Newkome, G. R.; Moorefield, C. N.; Vögtle, F. *Dendritic Molecules. Concepts, Syntheses, Perspectives*; VCH: Weinheim, Germany, 1996.

- (3) Bosman, A. W.; Janssen, H. M.; Meijer, E. W. *Chem. Rev.* **1999**, *99*, 1665–1688.
- (4) de Gennes, P.-G.; Hervet, H. J. *J. Phys. Lett. Fr.* **1983**, *44*, L351–L360.
- (5) Topp, A.; Bauer, B.; Klimash, J. W.; Spindler, R.; Tomalia, D. A.; Amis, E., *J. Macromolecules* **1999**, *32*, 7226–7231.
- (6) Lyuulin, A. V.; Davies, G. R.; Adolf, D. B. *Macromolecules* **2000**, *33*, 6899–6900.
- (7) Wooley, K. L.; Klug, C. A.; Tasaki, K.; Schaefer, J. *J. Am. Chem. Soc.* **1997**, *119*, 53–58.
- (8) Gorman, C. B.; Hager, M. W.; Parkhurst, B. L.; Smith, J. C. *Macromolecules* **1998**, *31*, 815–822.
- (9) (a) Chai, M.; Niu, Y.; Youngs, W. J.; Rinaldi, P. *Macromolecules* **2000**, *33*, 5395–5398. (b) Chai, M.; Niu, Y.; Youngs, W. J.; Rinaldi, P. *L. J. Am. Chem. Soc.* **2001**, *123*, 4670–4678.
- (10) Lescanec, R.; L., Muthukumar, M. *Macromolecules* **1992**, *25*, 2401.
- (11) Murat, M.; Grest, G. S. *Macromolecules* **1996**, *29*, 1278–1285.
- (12) Mansfield, M. L.; Klushin, L. I. *Macromolecules* **1993**, *26*, 4262–4268.
- (13) Mansfield, M. L. *Macromolecules* **2000**, *33*, 8043–8049.
- (14) Boris, D.; Rubinstein, M. *Macromolecules* **1996**, *29*, 7251–7260.
- (15) Ganazzoli, F.; La Ferla, R.; Terragni, G. *Macromolecules* **2000**, *33*, 6611–6620.
- (16) Mayo, S. L.; Olafson, B. D.; Goddard, W. A., III. *J. Phys. Chem.* **1990**, *94*, 8897–8909.
- (17) Theodorou, D. N.; Suter, U. W. *Macromolecules* **1985**, *18*, 1206–1214.
- (18) Lach, C.; Brizzolara, D.; Frey, H. *Macromol. Theory Simul.* **1997**, *6*, 371–380.
- (19) Zhang, H.; Grim, P. C. M.; Foubert, P.; Vosch, T.; Vanoppen, P.; Wiesler, U.-M.; Berresheim, A. J.; Muelken, K.; De Schryver, F. C. *Langmuir* **2000**, *16*, 9009–9014.
- (20) Scherrenberg, R.; Coussens, B.; van Vliet, P.; Edouard, G.; Brackman, J.; de Brabander, E. *Macromolecules* **1998**, *31*, 456–461.
- (21) Boris, D.; Rubinstein, M. *Macromolecules* **1996**, *29*, 7251–7260.
- (22) Lue, L. *Macromolecules* **2000**, *33*, 2266–2272.
- (23) Gorman, C. B.; Smith, J. C. *Polymer* **2000**, *41*, 675–683.
- (24) Mansfield, M. L. *Polymer* **1994**, *35*, 1827–1830.
- (25) Chen, Z. Y.; Cui, S.-M. *Macromolecules* **1996**, *29*, 7943–7952.
- (26) Wiener, H. *J. Am. Chem. Soc.* **1947**, *69*, 17–20.
- (27) La Ferla, R. *J. Chem. Phys.* **1997**, *106*, 688–700.
- (28) Diudea, M. V.; Pârv, B. *J. Chem. Inf. Comput. Sci.* **1995**, *35*, 1015–1018.

MA010953X